Deutscher Luft- und Raumfahrtkongress 2008
DocumentID: 81235

APPLICATION OF A CORRELATION-BASED INTERMITTENCY TRANSITION MODEL FOR HYPERSONIC FLOWS

M. Krause, Chair For Computational Analysis of Technical Systems (CATS),
J. Ballmann, Prof. Department of Mechanics,
RWTH Aachen University, Theaterplatz 14, D-52062 Aachen, Germany

Abstract

Within the frame of the GRK 1095 (Research Training Group) "Aero-Thermodynamic Design of a Scramjet Engine for Future Space Transportation Systems" a numerical and experimental analysis of hypersonic intake configurations has been initiated at RWTH Aachen University. The paper presents an overview of the ongoing work on the numerical simulations using a well validated Reynolds averaged Navier-Stokes solver, namely QUADFLOW.

For the simulations the γ - Re_θ model proposed by Langtry/Menter extended with alternate correlations for onset and length of transition is applied. For validation purpose, several simulations of subsonic flat plate flows and hypersonic double ramp configurations have been performed. The validation with respect to scramjet intakes is done by comparing the numerical results of this paper to experimental results of DLR Cologne.

Nomenclature

k	Turbulent kinetic energy
Re_x	Reynolds number, $\rho u_\infty x / \mu_\infty$
Re_θ	Momentum thickness Reynolds number, $\rho \theta U_0 / \mu$
$\mathrm{Re}_{\theta t}$	Transition onset momentum thickness Reynolds number, $\rho \theta_t U_0 / \mu$
$\overline{\mathrm{Re}_{\theta t}}$	Local transition onset momentum thickness Reynolds number
R_T	Viscosity ratio
R_y	Wall-distance based turbulent Reynolds number
R_v	Vorticity Reynolds number
S	Absolute value of strain rate, $(2 S_{ij} S_{ij})^{1/2}$
S_{ij}	Strain rate tensor, $0.5(\partial u_i / \partial x_j + \partial u_j / \partial x_i)$
U	Local velocity
u_∞	Inlet free stream velocity
y	Distance to nearest wall
θ	Momentum thickness
λ_θ	Pressure gradient parameter
μ	Molecular viscosity
μ_t	Eddy viscosity
Ω	Absolute value of vorticity, $(2 \Omega_{ij} \Omega_{ij})^{1/2}$
Ω_{ij}	Vorticity tensor, $0.5(\partial u_i / \partial x_j - \partial u_j / \partial x_i)$
ω	Specific turbulence dissipation rate

1. INTRODUCTION

The numerical prediction of laminar to turbulent transition and the prediction of relaminarisation are two of the most challenging and important aspects in flow simulation today. They can be found in a lot of working fields, like turbo-machinery and airplane design or hypersonic flow. There is a variety of transition mechanisms to be dealt with for creating a mathematical model to describe the transition process. In flows with low free stream turbulence mostly natural transition occurs due to Tollmien-Schlichting waves in the boundary layer (BL). In applications with higher free stream turbulence (e.g. more than 1 %) transition is generated by turbulent spots that are directly produced in the BL via free stream disturbances. This phenomenon is called Bypass-Transition. For flow conditions where separation bubbles occur, disturbances in the shear layer above these bubbles can cause laminar to turbulent transition. In hypersonic regimes shocks are generating turbulence so that they can also force a transition mechanism. A strong acceleration or cooling of the boundary layer can lead to a relaminarisation process, where the turbulent boundary layer becomes more or less laminar again.

To describe all these phenomena numerically an appropriate approach would probably be Detached Eddy Simulation (DES) or Direct Numerical Simulations (DNS). But these methods need extensive computational effort. So they are not appropriate for big test cases or problems of practical relevance.

For those problems RANS methods are still the best accessible way to model laminar to turbulent transition for industrial applications. In recent time the transition process is mostly described by an intermittency parameter γ, which provides the information about the fraction of time, when the flow is turbulent. The first who introduced the intermittency factor γ were Dhawan/Narashima [7].

Since this time a lot of approaches came up to numerically predict the transition process, for example: Steelant/Dick [8], [9] introduced conditioned averaged Navier Stokes equations, where the intermittency factor was also introduced in the momentum and energy equations, or Suzen/Huang [10], [11] who introduced a convection-diffusion equation for the intermittency factor. But all these models have the disadvantage of being dependent on integral values that have to be computed in the boundary layer and/or the whole solution domain. That is why these models can not be easily combined with parallel CFD codes. On the other hand parallel computing is essential for today's industrial applications.

The γ-Re_θ model proposed by Langtry/Menter [1], [2] overcomes this difficulty by predicting transition only by the use of local quantities. That is why it can easily be implemented in parallel Reynolds-averaged CFD codes. Nevertheless some problems remain. One is that the model is not completely published in literature. Two essential correlations for the prediction of transition onset and transition length are not explicitly given.

Within this paper alternate correlations will be presented for the transition onset and length. The paper also contains a description of Menters model and how the missing correlations have been replaced. The validation was done with respect to subsonic flat plate flows [3], [4] and hypersonic double ramp flows [5] as well as a scramjet intake configuration investigated at DLR Cologne [6].

The engine inlet of the considered air breathing hypersonic propulsion system consists of several exterior compression ramps followed by a subsequent interior isolator/diffuser assembly. A series of oblique shock waves are performing the compression of the incoming gas. The interaction of these strong shock waves with thick hypersonic boundary layers (BL) causes large separation zones that are responsible for a loss of mass flow and several other effects, like shock movement and high heat flux into the structure of the engine. The high total enthalpy of the flow yields severe aerodynamic heating, further enhanced by turbulent heat flux. All these flow phenomena can cause laminar to turbulent transition.

The performance of a scramjet intake is essential for the whole engine efficiency. That is why it is of great importance to model transition. It can occur on the first ramp (natural transition), at the kink between the ramps or on the second ramp (separation or shock induced transition). This depends on the geometrical design of the intake and the flow conditions. As an example for the intakes investigated within this project, transition occurs in the shear layer above the separation bubble between the two ramps of the intake. Additionally relaminarisation takes place while redirecting the flow into horizontal direction by the expansion over a convex ramp corner or a convex ramp shoulder within the intake.

The γ-Re_θ model in combination with the alternate correlations that are presented hereafter, try to provide a tool to predict transition in subsonic and hypersonic flow regimes.

2. THE FLOW SOLVER - QUADFLOW

The results of the computations shown within this paper were performed using the QUADFLOW code. It solves the unsteady Navier-Stokes equations for compressible fluid flow using a cell--centred finite volume method on unstructured grids. It has been developed within the SFB 401 (Collaborative Research Centre *"Flow Modulation and Fluid-Structure Interaction at Airplane Wings"*) and the GRK 5 (Research Training Group *"Transport Processes in Hypersonic Flows"*) at RWTH Aachen University and is still undergoing enhancement. QUADFLOW uses an integral concept of flow solver, multi-scale-analysis and local grid refinement [12]-[14]. So far, several implementations of turbulence models are validated and tested for 2D and 3D calculations, for example Spalart-Allmaras, LEA, SST, $k-\omega$. The code uses a fully implicit time integration via Newton-Krylov-method.

The computations are done on the SunFire SMP--cluster of RWTH Aachen University and the Jump cluster of Research Centre Jülich using MPI, based on the PETSc software.

3. TRANSITION MODEL DESCRIPTION

The model proposed in this paper is the γ-Re_θ model by Langtry/Menter [1], [2] augmented by alternate correlations for transition onset and length. The basis for the transition model is the SST model from Menter [15].

Additionally to the SST model there are two more transport equations to model the transition. The first one is the γ-intermittency equation used to trigger the transition process and to control the production of the turbulent kinetic energy in the BL. The second transition transport equation is formulated in terms of the transition onset

Reynolds number $\mathrm{Re}_{\theta t}$ that is used to capture the non-local effect of free stream turbulence intensity and pressure gradient at the BL edge.

3.1. γ - Intermittency Equation

The intermittency equation is formulated as follows:

$$\frac{\partial(\rho\gamma)}{\partial t}+\frac{\partial(\rho U_j\gamma)}{\partial x_j}= P_\gamma - E_\gamma + \frac{\partial}{\partial x_j}\left[\left(\mu+\frac{\mu_t}{\sigma_f}\right)\frac{\partial\gamma}{\partial x_j}\right] \tag{1}$$

The transition source term is defined as:

(2) $P_\gamma = F_{length} c_{a1}\rho S[\gamma F_{onset}]^{0.5}(1-c_{e1}\gamma)$,

where S is the strain rate magnitude, $c_{e1}=1.0$, $c_{a1}=2.0$, $\sigma_f=1.0$. The function F_{onset} triggers the intermittency production and is formulated as follows:

(3) $F_{onset}=\max(F_{onset2}-F_{onset3}, 0.0)$,

(4) $F_{onset2}=\min\left(\max\left(F_{onset1}, F_{onset1}{}^4\right), 2.0\right)$,

with

(5) $F_{onset1}=\dfrac{\mathrm{Re}_v}{2.193\cdot \mathrm{Re}_{\theta c}}$, $\mathrm{Re}_v=\dfrac{\rho y^2 S}{\mu}$,

where Re_v is the vorticity Reynolds number. F_{onset3} is defined in terms of the viscosity ratio as follows:

(6) $F_{onset3}=\max\left(1-\left(\dfrac{R_T}{2.5}\right)^3, 0.0\right)$, $R_T=\dfrac{\rho k}{\mu\omega}$.

The $\mathrm{Re}_{\theta c}$ of eq. (5) is the critical Reynolds number where the intermittency first starts to increase in the BL. It is defined as:

(7) $\mathrm{Re}_{\theta c}=f\left(\overline{\mathrm{Re}_{\theta t}}\right)$.

This is the correlation used for transition onset and is not explicitly given by Langtry/Menter. The alternate formulation of $\mathrm{Re}_{\theta c}$ will be given in chapter 4.

The function F_{length} is the correlation for transition length, which is also not given in [1], [2]. It is defined as:

(8) $F_{length}=f\left(\overline{\mathrm{Re}_{\theta t}}\right)$,

and its ansatz used in this paper will also be given as alternate correlation in chapter 4.

The destruction/relaminarisation source is defined as follows:

(9) $E_\gamma = c_{a2}\rho\Omega\gamma F_{turb}(c_{e2}\gamma-1)$, $F_{turb}=e^{-\left(\frac{R_T}{4}\right)^4}$,

where Ω is the vorticity magnitude, $c_{a2}=0.06$ and $c_{e2}=50.0$.

The boundary condition for γ at free side boundary is zero normal flux while for inflow and free stream the value is set equal to one, and at no-slip walls γ is set to zero.

3.2. Transport Equation for Transition Momentum Thickness Reynolds Number

The transport equation is defined as follows:

$$\frac{\partial\left(\rho\overline{\mathrm{Re}_{\theta t}}\right)}{\partial t}+\frac{\partial\left(\rho U_j\overline{\mathrm{Re}_{\theta t}}\right)}{\partial x_j}= P_{\theta t}+\frac{\partial}{\partial x_j}\left[\sigma_{\theta t}(\mu+\mu_t)\frac{\partial\overline{\mathrm{Re}_{\theta t}}}{\partial x_j}\right] \tag{10}$$

with the source term:

(11) $P_{\theta t}=c_{\theta t}\dfrac{\rho}{t}\left(\mathrm{Re}_{\theta t}-\overline{\mathrm{Re}_{\theta t}}\right)(1.0-F_{\theta t})$,

where $c_{\theta t}=0.03$, $\sigma_{\theta t}=2.0$ and t is a time scale for dimensional reasons and defined as:

(12) $t=\dfrac{500\mu}{\rho U^2}$.

$\mathrm{Re}_{\theta t}$ is the transition onset Reynolds number and is defined by experimental correlations given by Langtry/Menter [1]. $F_{\theta t}$ is a blending function that is used to turn off the source term in the BL and to allow the transported scalar $\overline{\mathrm{Re}_{\theta t}}$ to diffuse in from the free stream. It is defined as follows:

(13) $F_{\theta t}=\min\left(\max\left(F_{wake}e^{-\left(\frac{y}{\delta}\right)^4}, 1.0-\left(\dfrac{\gamma-1/c_{e2}}{1.0-1/c_{e2}}\right)^2\right), 1.0\right)$

The functions F_{wake} and δ are given as follows:

(14) $F_{wake}=e^{-\left(\frac{\mathrm{Re}_\omega}{1\cdot 10^5}\right)^2}$, $\mathrm{Re}_\omega=\dfrac{\rho\omega y^2}{\mu}$,

(15) $\delta=\dfrac{50\Omega y}{U}\cdot\delta_{BL}$, $\delta_{BL}=\dfrac{15}{2}\theta_{BL}$, $\theta_{BL}=\dfrac{\overline{\mathrm{Re}_{\theta t}}\mu}{\rho U}$

The boundary condition for $\overline{\mathrm{Re}_{\theta t}}$ at walls is zero normal flux. According to Langtry/Menter for an inflow boundary it is computed from the empirical correlation based on the inlet turbulence intensity. Within this paper, $\overline{\mathrm{Re}_{\theta t}}=0.001$ at no-slip walls and the inflow was used, because this leaded to a faster convergence of the solution.

3.3. Empirical Correlation for Transition Onset Reynolds Number $\mathrm{Re}_{\theta t}$

The empirical correlation for the transition onset Reynolds number is defined differently for low turbulence and high turbulence intensities as follows:

(16) $$\mathrm{Re}_{\theta t} = \left[1173.51 - 589.428Tu + \frac{0.2196}{Tu^2}\right] \cdot F(\lambda_\theta),$$

for $Tu \le 1.3$,

(17) $$\mathrm{Re}_{\theta t} = 331.5 \cdot [Tu - 0.5658]^{-0.671} \cdot F(\lambda_\theta),$$

for $Tu > 1.3$, with the function

(18) $$F(\lambda_\theta) = 1 - \left[-12.986\lambda_\theta - 123.66\lambda_\theta^2 - 405.689\lambda_\theta^3\right] \cdot e^{-\left[\frac{Tu}{1.5}\right]^{1.5}},$$

for $\lambda_\theta \le 0.0$ and

(19) $$F(\lambda_\theta) = 1 + 0.275 \cdot \left[1 - e^{-35.0\lambda_\theta}\right] \cdot e^{-\left[\frac{Tu}{0.5}\right]},$$

for $\lambda_\theta > 0.0$, where the Tu is the turbulence intensity which is given as:

(20) $$Tu = 100 \cdot \frac{\sqrt{2k/3}}{U}.$$

The pressure gradient parameter λ_θ is defined as:

(21) $$\lambda_\theta = \frac{\rho\theta^2}{\mu}\frac{dU}{ds},$$

where dU/ds is the acceleration in stream wise direction and can be computed as follows:

(22) $$U = \left(u^2 + v^2 + w^2\right)^{\frac{1}{2}},$$

(23) $$\frac{dU}{dx} = U^{-1} \cdot \left[u\frac{du}{dx} + v\frac{dv}{dx} + w\frac{dw}{dx}\right],$$

(24) $$\frac{dU}{dy} = U^{-1} \cdot \left[u\frac{du}{dy} + v\frac{dv}{dy} + w\frac{dw}{dy}\right],$$

(25) $$\frac{dU}{dz} = U^{-1} \cdot \left[u\frac{du}{dz} + v\frac{dv}{dz} + w\frac{dw}{dz}\right],$$

(26) $$\frac{dU}{ds} = \left[(u/U)\frac{dU}{dx} + (v/U)\frac{dU}{dy} + (w/U)\frac{dU}{dz}\right].$$

The equations (16) to (19) have to be solved iteratively together with eq. (21) and the eq. $\theta = \mathrm{Re}_{\theta t} \cdot \mu / (\rho U)$. The authors of this paper suggest for the initial value $\theta = 0.0$. This leaded to a fast convergence within less then 10 iterations.

3.4. Coupling of the Transition Model with the SST Turbulence Model

As mentioned above the transition model is used in combination with the SST model from Menter [15] so that only minor changes in the production and destruction term of the k - equation have to be done. The equation for ω is unaltered.

The production term of the k-equation is modified as follows:

(27) $$P_{k\_new} = \gamma_{eff} \cdot P_{k\_orig},$$

and the destruction term is defined as:

(28) $$D_{k\_new} = \min\left(\max\left(\gamma_{eff}, 0.1\right), 1.0\right) \cdot D_{k\_orig},$$

with

(29) $$\gamma_{eff} = \max(\gamma, \gamma_{sep}),$$

(30) $$\gamma_{sep} = \min\left(s_1 \max\left[0, \left(\frac{\mathrm{Re}_v}{3.235\,\mathrm{Re}_{\theta c}}\right) - 1\right] F_{reattach}, 2\right) \cdot F_{\theta t},$$

where $s_1 = 2.0$ and

(31) $$F_{reattach} = e^{-\left(\frac{R_T}{20.0}\right)^4}.$$

Some final modifications have to be done for the blending function F_1 of the original SST model and these are defined as:

(32) $$F_{1new} = \max\left(F_{1orig}, F_3\right),$$

with

(33) $$F_3 = e^{-\left(\frac{R_y}{120.0}\right)^8}, \quad R_y = \frac{\rho y \sqrt{k}}{\mu}.$$

4. ALTERNATE CORRELATIONS FOR TRANSITION ONSET AND LENGTH

In this chapter the evaluation of the alternate correlations for transition onset and length will be shown, first for subsonic flow regime and second for hypersonic flow regime.

4.1. Subsonic Flow

To determine the missing correlations various numerical simulations of flat plate test cases were performed. For validation the test cases of the ERCOFTAC database and the Schubauer/Klebanoff test case were taken. These are commonly used as benchmark for verification of transition models and are denoted as T3A, T3A-, T3B, T3C1, T3C2, T3C3, T3C4, T3C5 and Schubauer/Klebanoff (S/K). The first 3 test cases and the one from S/K are characterized by a zero pressure gradient flow, while the other ones are characterized by an adverse/favourable pressure gradient.

As mentioned before the transition onset and length are functions of $\overline{\mathrm{Re}_{\theta t}}$, see eq. (7) and (8). That is why a certain factor had to be introduced to investigate the influence of the $\overline{\mathrm{Re}_{\theta t}}$ on the transition onset. In the following this factor will be called f_{trans}. In accordance with Langtry/Menter the critical Reynolds number $\mathrm{Re}_{\theta c}$ (where the intermittency first starts to increase in the BL) is reached upstream of the transition Reynolds number $\mathrm{Re}_{\theta t}$. This is due to the fact that turbulence first has to build up within the boundary layer. So there is a certain delay between start of intermittency increase and the point of transition. To evaluate the connection between these two Reynolds numbers the authors started with setting $\mathrm{Re}_{\theta c} = \overline{\mathrm{Re}_{\theta t}}$. Then the factor f_{trans} was introduced to investigate the behaviour of the model.

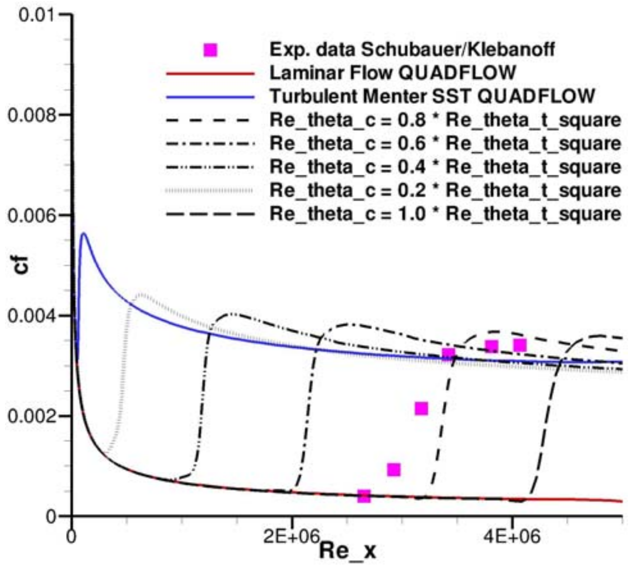

BILD 1. Schubauer/Klebanoff test case, flow conditions table (1), $F_{length} = 1$

To show the dependence of transition onset on $\mathrm{Re}_{\theta c}$, BILD (1) (S/K test case) and BILD (2) (T3C1 test case) are presenting the friction coefficient in comparison to the experimental data. The S/K test case has very low free stream turbulence intensity $Tu_\infty = 0.18\%$ and is a zero pressure gradient flow, while the T3C1 case has high free stream turbulence intensity $Tu_\infty = 6.6\%$ and is characterized by an adverse pressure gradient.

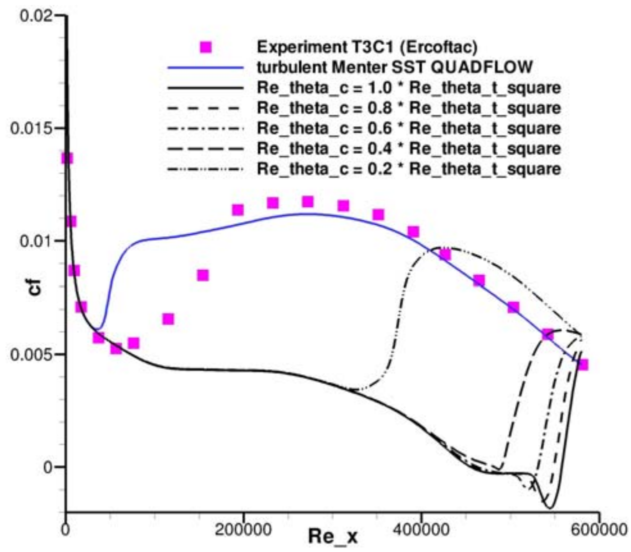

BILD 2. T3C1 test case, flow conditions table (1), $F_{length} = 1$

It has to be mentioned, that the initial conditions for the turbulence quantities are influencing the transition point. Within this work the initial conditions for the turbulence kinetic energy k_∞ and the ω_∞ where set according to Menter [15] to:

$$k_\infty = 1.5(Tu_\infty u_\infty \cdot 0.01)^2 \qquad \omega_\infty = \frac{\rho_\infty k_\infty}{\mu_{t\infty}}. \tag{34}$$
$$\mu_{t\infty} = 0.001 \cdot \mu_\infty$$

This is different to the assumptions Langtry/Menter made while computing the flat plate test cases. There the turbulence intensity at infinity varies together with the ratio of $\mu_{t\infty}/\mu_\infty$. The authors of this paper wanted to reduce the number of input parameters that influence the transition process. That is why the correlations were found with a constant ratio of $\mu_{t\infty}/\mu_\infty$ like seen in eq. (34).

In BILD (1) and BILD (2) the value of F_{length} was set to 1. It can be seen that with a linear decrease of the factor f_{trans} the transition point is nonlinearly moving in more upstream direction (the x-coordinate Re_x was defined with the infinity free stream velocity for both test cases). The transition length remains unchanged. Additionally, it can be observed that the behaviour of the transition model is not the same for the S/K test case and the T3C1 test case. When the inflow turbulence intensity increases, the factor f_{trans} has to be decreased, to get an appropriate result. By comparing these two test cases it was found, that the maximum difference of $\overline{\mathrm{Re}_{\theta t}}$ was only 0.8 %. That is why the authors decided to take the inflow turbulence as an additional factor for determining the value of $\mathrm{Re}_{\theta c}$. This leads to the following correlation for the transition onset in subsonic regime:

(35) $$\mathrm{Re}_{\theta c} = \frac{\overline{\mathrm{Re}_{\theta t}}}{\left(-0.042 \cdot Tu_\infty^3 + 0.4233 \cdot Tu_\infty^2 + 0.0118 \cdot Tu_\infty + 1.0744\right)}.$$

As mentioned before, the parameters F_{length} and $\mathrm{Re}_{\theta c}$ are not independent of each other. That is why in the following the variation of F_{length} is shown for a fixed $\mathrm{Re}_{\theta c}$. In BILD (3) (S/K test case) the value of F_{length} is shown for $\mathrm{Re}_{\theta c} = 0.8 \cdot \overline{\mathrm{Re}_{\theta t}}$. BILD (4) (T3C1) presents the value of F_{length} for $\mathrm{Re}_{\theta c} = 0.1 \cdot \overline{\mathrm{Re}_{\theta t}}$, respectively.

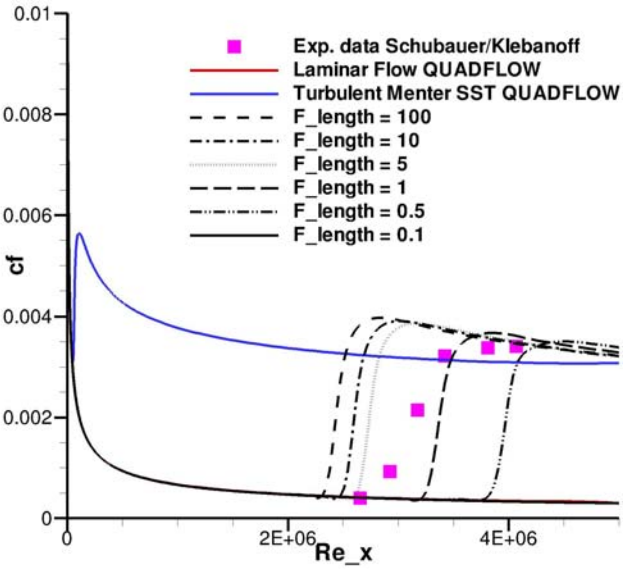

BILD 3. Schubauer/Klebanoff test case, flow conditions table (1), $\mathrm{Re}_{\theta c} = 0.8 \cdot \overline{\mathrm{Re}_{\theta t}}$

One can see that the factor F_{length} changes the transition point in a nonlinear way. An increasing of it leads to an upstream movement of the transition point. For small turbulence intensities like in the S/K test case the value of F_{length} has only minor influence on the transition length. This is different for higher turbulence intensities like shown in the T3C1 test case in BILD (4). It can also be pointed out that the influence on the transition point for very high numbers of F_{length} is very small. For this reason the authors suggest a range for F_{length} from 0.1 to 100 for subsonic regime, it will be shown in chapter 4.2 that this is different for hypersonic flow regime. Choosing a higher value then 100 would have a negligible influence on the transition length and onset.

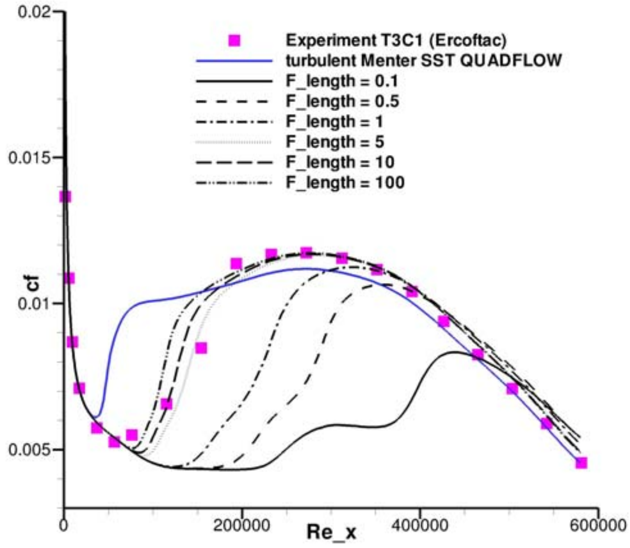

BILD 4. T3C1 test case, flow conditions table (1), $\mathrm{Re}_{\theta c} = 0.1 \cdot \overline{\mathrm{Re}_{\theta t}}$

Because of the less influence of F_{length} on the transition length for low turbulence intensities it was decided to split the alternate correlation into two parts, again depending on the turbulence intensity at minus infinity. F_{length} is described in the following:

(36) $$F_{length} = \frac{\ln\left(\overline{\mathrm{Re}_{\theta t}} + 1\right)}{Tu_\infty}, \quad Tu_\infty \le 1.0\%.$$

(37) $$F_{length} = \ln\left(\overline{\mathrm{Re}_{\theta t}} + 1\right) \cdot \left(0.2337 Tu_\infty^2 - 1.3493 Tu_\infty + 2.1449\right), \quad Tu_\infty > 1.0\%$$

4.2. Hypersonic Flow

Due to the high vorticity production through non-planar shock waves and in regions of stagnation some corrections for hypersonic flow were made to the correlations. Additionally the value of $\overline{\mathrm{Re}_{\theta t}}$ within the hypersonic flow regime is much higher than in the subsonic flow. Several spots in the flow field (e.g. reattachment zones) can easily reach values of $\overline{\mathrm{Re}_{\theta t}} = 1 \cdot 10^5$, while in subsonic regimes $\overline{\mathrm{Re}_{\theta t}}$ reaches only about 2% of this value. That is why the authors decided to replace the value of $\overline{\mathrm{Re}_{\theta t}}$ in the correlations by the turbulence intensity at infinity Tu_∞. These changes were proven by double ramp hypersonic flow test cases [5] and scramjet intake test cases [6], see chapter 5.2.

The corrected correlations for hypersonic flow regimes are defined as follows:

(38) $\mathrm{Re}_{\theta c} = 967.34 \cdot Tu_\infty^{-1.0315}$ and

(39) $F_{length} = 10.435 \cdot Tu_\infty^{2.9756}$.

It was found that in hypersonic flow regimes the factor F_{length} must be smaller than in the subsonic case. A factor above 1 leaded to nearly fully turbulent solutions. That is why the factor F_{length} should be in the range of 10^{-3} to 1. In the contrary the factor of $\mathrm{Re}_{\theta c}$ should be increased to get appropriate results. An increasing $\mathrm{Re}_{\theta c}$ and decreasing F_{length} lead to a more laminar behaviour of the transition model which corresponds to the higher turbulence production within hypersonic flow regimes. For the hypersonic test cases investigated within this paper the value of Tu_{∞} was varied between 0.1 and 1.

5. RESULTS

5.1. Subsonic Flat Plate Test Cases

In this chapter some results for flat plate test cases with and without adverse pressure gradient are presented. The inlet conditions for the various cases can be found in table (1).

The computational grids had a total of 96 points in y-direction and 540 points in x-direction with a minimum resolution of $1 \cdot 10^{-6}$ m at the leading edge in both x- and y- direction. This leaded to a y^{+} value below 1.0.

case	$\frac{dp}{dx}$	u_{∞} [m/s]	Tu_{∞} [%]	μ [kg/ms]	k [m²/s²]	ω [10³/s]
S/K	zero	50.1	0.18	1.86E-5	0.0122	803
T3A-	zero	19.8	0.87	1.86E-5	0.0449	2958
T3A	zero	5.4	3.5	1.86E-5	0.0536	3529
T3B	zero	9.4	6.5	1.86E-5	0.56	36881
T3C1	var.	5.9	6.6	1.86E-5	0.2275	14980

TAB 1. Inlet conditions for flat plate test cases

The BILDer (5) – (8) are showing the friction coefficient of the steady state flat plate test cases with zero pressure gradient. The black lines are the theoretical solutions for a laminar (Blasius solution) and turbulent boundary layer, respectively. The blue lines denote the fully turbulent solution with the in-house code QUADFLOW using the low Reynolds Version of the standard Menter SST Model [15]. The red lines are the laminar solutions.

It can be seen that the location of transition onset is predicted quite accurately for all cases. Differences for the length of laminar to turbulent transition occur for low free stream turbulence intensities (S/K and T3A- test cases). Here the predicted length is to short which means that the transition model makes grow the turbulence to fast within the boundary layer.

For the cases with higher free stream turbulence intensities the predicted transition length is correct.

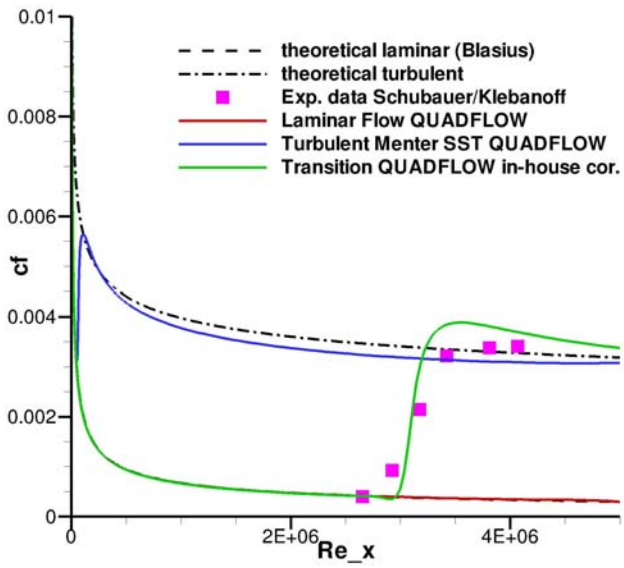

BILD 5. Schubauer/Klebanoff. test case

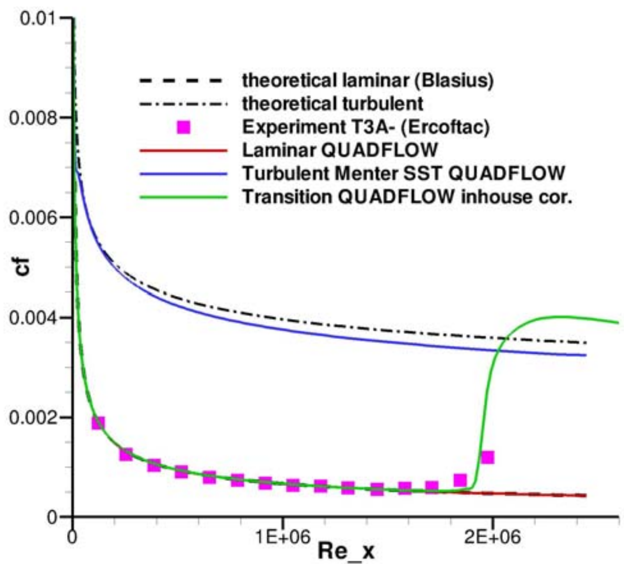

BILD 6. T3A- test case

BILD (9) shows the friction coefficient of a steady state flat plate test case with adverse pressure gradient. It can be seen that the length of transition is predicted a little too short and the onset point is little downstream of the experimental one. Nevertheless the computational result fits well to the experiment.

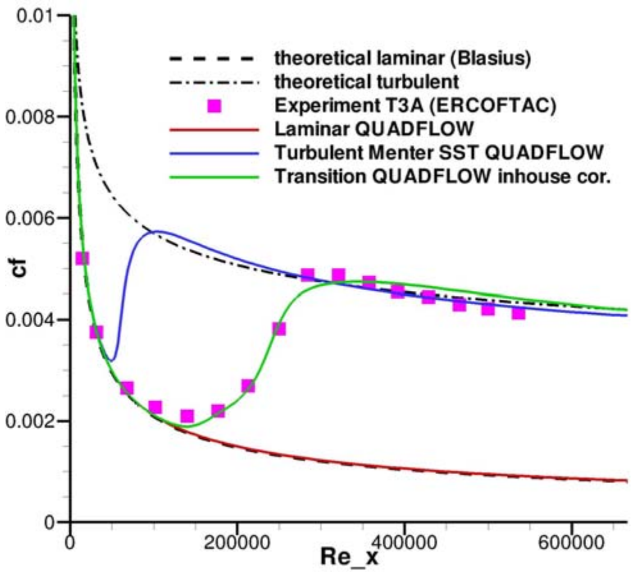

BILD 7. T3A test case

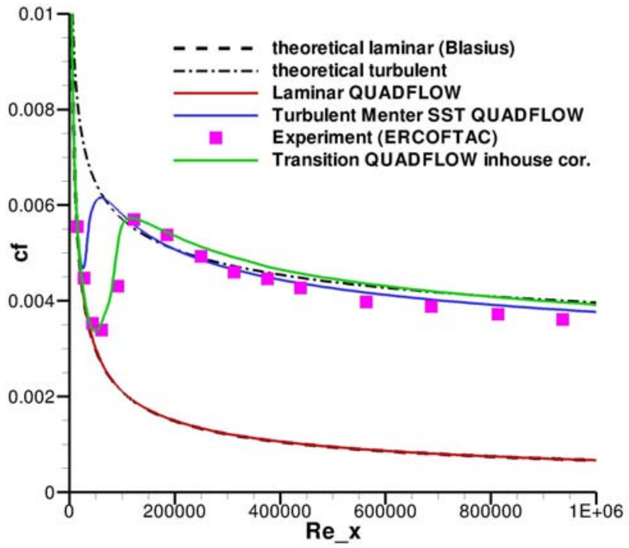

BILD 8. T3B test case

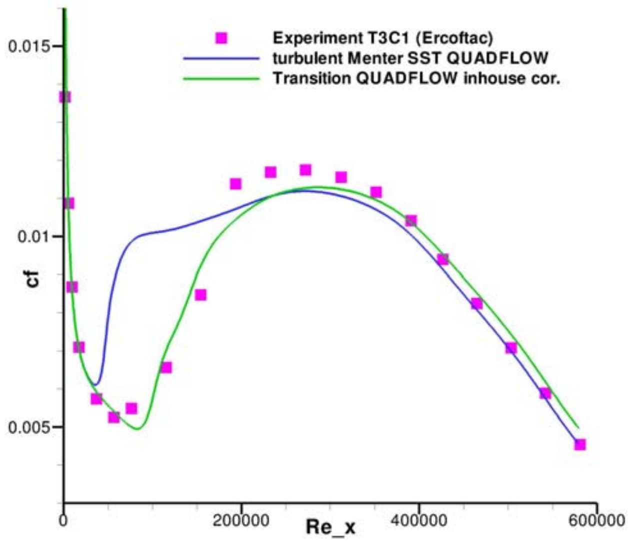

BILD 9. T3C1 test case

5.2. Hypersonic Double Ramp Test Cases

In the following, four test cases with two different hypersonic double ramp configurations are shown which were investigated experimentally [5]. The first ramp has an angle of $9°$ and the second one of $20.5°$. The length of the first ramp is 180 mm, of the second one 250 mm. The width is 200 mm. The first configuration has a sharp leading edge; the second one has a blunt leading edge radius of 0.5 mm. The computed results shown are 2D calculations. The flow conditions are as follows: $Ma = 8.3$, $T_\infty = 102K$, $\rho_\infty = 0.0158\,kg/m^3$, $\mathrm{Re} = 3.76 \cdot 10^5$. Comparing the experimental results with the computational ones an offset in the pressure coefficient can be found. This offset is due to small differences in the free stream conditions, because the inflow conditions in front of the model geometry in a shock tube suffer always from a little uncertainty. Additionally in the computations the same inflow conditions were used for every case, which can not be assured for experimental investigations. One reason for differences at the higher wall temperature can be the temperature distribution on the model surface. In the experiment it is not constant. At the leading edge and the sides of the ramps the model was not heated. Additionally some differences can be due to some side flow that occurs in the experiment, but can not be captured in 2D computations.

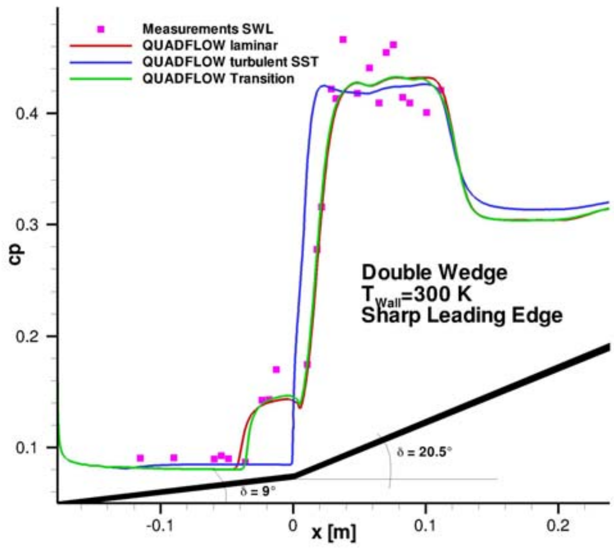

BILD 10. Hypersonic double ramp, sharp leading edge

BILDer (10) – (13) are showing the pressure coefficient for $T_{Wall} = 300K$ and $T_{Wall} = 600K$. Again the red lines are indicating the laminar solution, the blue lines the turbulent one with the Menter SST Model and the green ones the transition model. One can see that a laminar solution overestimates the size of the separation, while the fully turbulent one does not show any separation. The transitional solution predicts the pressure coefficient very well. It can be stated that the separation bubble in the kink between the ramps is growing with increasing wall temperature. Additionally the separation zone is bigger in case of the blunt leading edge. Both effects were predicted correctly by the transition model and the correlations used. For a detailed description of these effects see [5], [16] and [17].

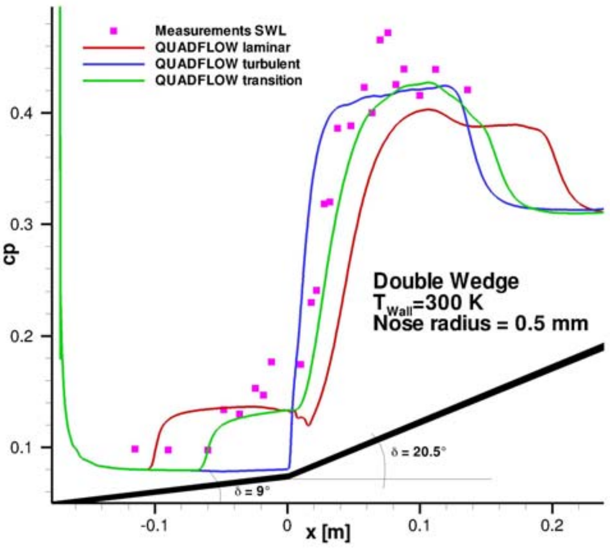

BILD 11. Hypersonic double ramp, round leading edge

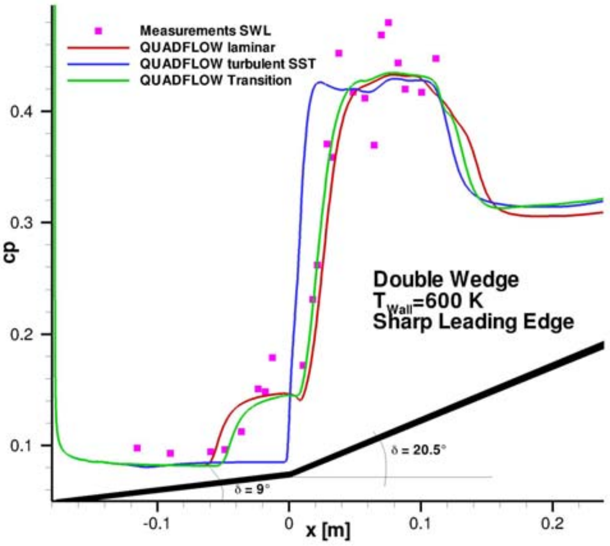

BILD 12. Hypersonic double ramp, sharp leading edge

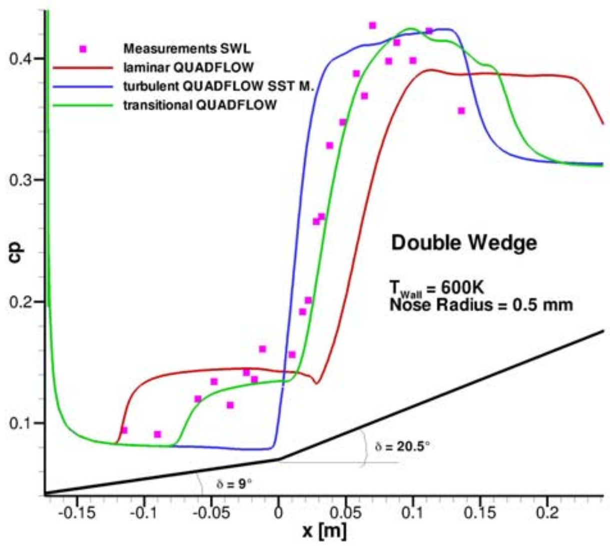

BILD 13. Hypersonic double ramp, round leading edge

Furthermore, BILD (14) shows the Stanton number distribution for the test case with blunt leading edge and a wall temperature of 300 K. The Stanton number strongly increases when the transition from laminar to turbulent takes place, thus the heat flux into the structure increases, too. Therefore, it is of great importance to predict the transition point correctly for hypersonic configurations.

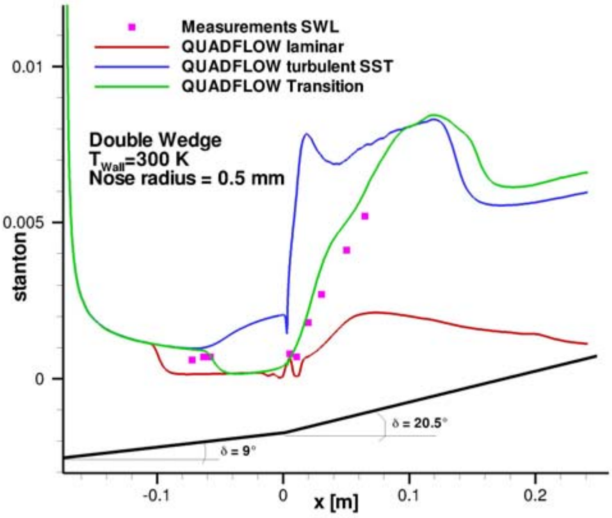

BILD 14. Hypersonic double ramp, round leading edge

5.3. Scramjet Intake Test Case

BILD (15) shows the Mach contours and the pressure distribution (on the ramp side) for a scramjet intake investigated at DLR Cologne [6]. Transition occurs in the shear layer above the separation bubble in the kink between the two ramps. The laminar BL on the first ramp separates and generates a separation shock. Behind this shock the BL becomes turbulent and reattaches on the second ramp, generating a reattachment shock. This effect can be seen in the pressure distribution. At the convex ramp shoulder the BL is accelerated and so the pressure coefficient decreases. Additionally the BL becomes partly laminar again. The shock from the cowl hits the ramp side BL and generates a separation bubble. This separation bubble creates a separation shock in front and a reattachment shock behind it. This can be also seen in the pressure distribution. The reattachment shock is reflected on the upper isolator wall. At this point a small separation occurs due to the interaction of the reflected shock with the turbulent BL at the cowl.

Looking at BILD (15) one can see that small differences between the numerical and experimental results remain. This can be due to the 2D numerical treatment. There are some effects that occur due to the sidewall BL (e.g. additional compression waves) that could not be modelled.

Finally it can be stated that for the hypersonic test cases presented within this paper the correlations found are working well. The next steps will be performing 3D computations of the scramjet intake test cases and do more investigations with different intake configurations and inflow conditions.

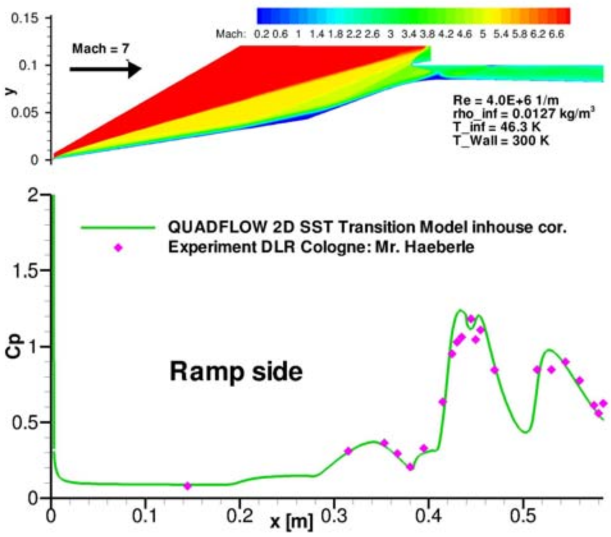

BILD 15. Intake GRK 1095, blunt leading edge

6. CONCLUSION

For supersonic combustion with resulting positive engine thrust, the performance of the intake is essential. That is why a combined investigation based on numerical analysis and experimental examination of scramjet intake geometries is undertaken. The numerical investigation is of great importance, because one aim of the research is to design a well-suited hypersonic intake for the given flight trajectory. Transition effects have great influence on the overall flow field in scramjet intake. To model the transition effects occurring, a transition model was studied.

Within this paper the results for flat plate, hypersonic double ramp as well as scramjet intake configurations are shown. The computations were performed with the QUADFLOW solver using the Langtry/Menter γ - Re_θ Transition Model in combination with alternate correlations for transition onset and length. This paper shows that the correlations found can be used in subsonic as well as in hypersonic/supersonic flow regimes.

The experimental work will allow validating the computational results, so that the numerical simulations can be used to investigate the flow behaviour more independently from experiments. In the near future the model will be used for 3D Scramjet intake configurations for further development of the correlations as well as to investigate the transition effects occurring in hypersonic intakes and to design a scramjet intake.

With the model description given in this paper it should be possible to implement the transition model in standard CFD RANS solvers.

7. ACKNOWLEDGMENTS

The authors want to thank the Deutsche Forschungsgesellschaft (DFG) for funding this project.

8. REFERENCES

[1] Langtry, R., “A Correlation-Based Transition Model using Local Variables for Unstructured Parallelized CFD Codes”, Ph.D. Thesis, Stuttgart University, 2006.

[2] Menter, F. and Langtry, R., “A Correlation-Based Transition Model Using Local Variables Part1 - Model Formulation,” Proceedings of ASME Turbo Expo, 2004, GT2004-53452.

[3] Schubauer, G. and Klebanoff, P., “Contributions on the Mechanics of Boundary Layer Transition,” NACA TN, Vol. 3489, 1955.

[4] Savill, A., “Some recent progress in the turbulence modeling of by-pass transition,” Near - Wall Turbulent Flows, 1993, pp. 829–839

[5] Neuenhahn, T. and Olivier, H., “Influence of the wall temperature and entropy layer effects on double wedge shock boundary layer interactions,” AIAA 2006-8136, 2006.

[6] Häberle, J. and Gülhan, A., “Investigation of the Flow Field of a 2D Scramjet Inlet at Mach 7 with optional Boundary Layer Bleed,” 43rd Joint Propulsion Conference and Exhibit , No. 2007-5068, 2007.

[7] Dhawan, S. and Narasimha, R., “Some properties of boundary layer during the transition from laminar to turbulent flow motion,” Journal of Fluid and Mechanics, Vol. 3, 1958, pp. 418–436.

[8] Steelant, J. and Dick, E., “Modeling of bypass transition with conditioned Navier-Stokes equations coupled to an intermittency transport equation,” International Journal on Numerical Methods in Fluids, Vol. 23, No. 3, 1996, pp. 193–220.

[9] Steelant, J. and Dick, E., “Modeling of laminar-turbulent transition for high free stream turbulence,” Journal of Fluids and Engineering, Vol. 123, No. 1, 2001, pp. 22–30.

[10] Suzen, Y. and Huang, P., “Modeling of flow transition using an intermittency transport equation,” Journal of Fluids Engineering, Vol. 122, No. 2, 2000, pp. 273–284.

[11] Suzen, Y., Xiong, G., and Huang, P., “Prediction of transitional flows in low-pressure turbines using an intermittency transport equation,” AIAA Journal, Vol. 40, No. 2, 2002, pp. 254–266.

[12] Bramkamp, F. D., Lamby, P., and Müller, S., “An adaptive multiscale finite volume solver for unsteady and steady flow computations,” Journal of Computational Physics, Vol. 197, 2004, pp. 460–490.

[13] Bramkamp, F., Gottschlich-Müller, B., Hesse, M., Lamby, P., Müller, S., Ballmann, J., Brakhage, K., and Dahmen, W., “H-Adaptive Multiscale Schemes for Compressible Navier-Stokes Equations - Polyhedral Discretization, Data Compression and Mesh Generation,” Notes on Numerical Fluid Mechanics and Multidisciplinary Design, Vol. 84, 2003, pp. 125–204.

[14] Bramkamp, F. D., Bücker, H. M., and Rasch, A., “Using Exact Jacobians in an Implicit Newton-Krylov Method,” Computers and Fluids, 35(10):1063-1073, 2005.

[15] Menter, F. R., “Two-Equation Eddy-Viscosity Turbulence Models for Engineering Applications,” AIAA Journal, Vol. 32, No. 8, Aug. 1994, pp. 1598–1605.

[16] Krause, M. and Ballmann, J., “Numerical Simulation and Design of a Scramjet Intake Using Two Different RANS Solvers,” 43rd Joint Propulsion Conference and Exhibit, No. 2007-5423, 2007.

[17] Krause, M., Reinartz, B., and Ballmann, J., “Numerical Computations for Designing a Scramjet Intake,” 25th ICAS Conference, 2006